

# Mechanism of the metallic metamaterials coupled to the gain material

Zhixiang Huang,<sup>1,2</sup> Sotiris Droulias,<sup>3\*</sup> Thomas Koschny,<sup>1</sup> and Costas M. Soukoulis<sup>1,3</sup>

<sup>1</sup>Department of Physics and Astronomy and Ames Laboratory, Iowa State University, Ames, Iowa 50011, USA

<sup>2</sup>Key Laboratory of Intelligent Computing and Signal Processing, Anhui University, Hefei 230039, China

<sup>3</sup>Institute of Electronic Structure and Laser, FORTH, 71110 Heraklion, Crete, Greece

\*sdroulias@iesl.forth.gr

**Abstract:** We present evidence of strong coupling between the gain material and the metallic metamaterials. It is of vital importance to understand the mechanism of the coupling of metamaterials with the gain medium. Using a four-level gain system, the numerical pump-probe experiments are performed in several configurations (split-ring resonators (SRRs), inverse SRRs and fishnets) of metamaterials, demonstrating reduction of the resonator damping in all cases and hence the possibility for loss compensation. We find that the differential transmittance  $\Delta T/T$  can be negative in different SRR configurations, such as SRRs on the top of the gain substrate, gain in the SRR gap and gain covering the SRR structure, while in the fishnet metamaterial with gain  $\Delta T/T$  is positive.

©2014 Optical Society of America

**OCIS codes:** (160.4760) Optical properties; (160.3918) Metamaterials; (260.5740) Resonance; (350.4238) Nanophotonics and photonic crystals.

---

## References and links

1. C. M. Soukoulis, S. Linden, and M. Wegener, "Physics. Negative refractive index at optical wavelengths," *Science* **315**(5808), 47–49 (2007).
2. C. M. Soukoulis and M. Wegener, "Materials science. Optical metamaterials—More bulky and less lossy," *Science* **330**(6011), 1633–1634 (2010).  
C. M. Soukoulis and M. Wegener, "Past achievements and future challenges in the development of three-dimensional photonic metamaterials," *Nat. Photonics* **5**, 523 (2011).
3. Y. Liu and X. Zhang, "Metamaterials: a new frontier of science and technology," *Chem. Soc. Rev.* **40**(5), 2494–2507 (2011).
4. A. Fang, T. Koschny, and C. M. Soukoulis, "Self-consistent calculations of loss-compensated fishnet metamaterials," *Phys. Rev. B* **82**(12), 121102 (2010).
5. S. Wuestner, A. Pusch, K. L. Tsakmakidis, J. M. Hamm, and O. Hess, "Overcoming losses with gain in a negative refractive index metamaterial," *Phys. Rev. Lett.* **105**(12), 127401 (2010).
6. O. Hess, J. B. Pendry, S. A. Maier, R. F. Oulton, J. M. Hamm, and K. L. Tsakmakidis, "Active nanoplasmic metamaterials," *Nat. Mater.* **11**(7), 573–584 (2012).
7. A. Fang, Z. Huang, Th. Koschny, and C. M. Soukoulis, "Overcoming the losses of a split ring resonator array with gain," *Opt. Express* **19**(13), 12688–12699 (2011).
8. Z. Huang, T. Koschny, and C. M. Soukoulis, "Theory of pump-probe experiments of metallic metamaterials coupled to a gain medium," *Phys. Rev. Lett.* **108**(18), 187402 (2012).
9. X. L. Zhong and Z. Y. Li, "All-analytical semiclassical theory of spaser performance in a plasmonic nanocavity," *Phys. Rev. B* **88**(8), 085101 (2013).
10. S. Xiao, V. P. Drachev, A. V. Kildishev, X. Ni, U. K. Chettiar, H.-K. Yuan, and V. M. Shalaev, "Loss-free and active optical negative-index metamaterials," *Nature* **466**(7307), 735–738 (2010).
11. E. Plum, V. A. Fedotov, P. Kuo, D. P. Tsai, and N. I. Zheludev, "Towards the lasing spaser: controlling metamaterial optical response with semiconductor quantum dots," *Opt. Express* **17**(10), 8548–8551 (2009).
12. K. Tanaka, E. Plum, J. Y. Ou, T. Uchino, and N. I. Zheludev, "Multifold Enhancement of Quantum Dot Luminescence in Plasmonic Metamaterials," *Phys. Rev. Lett.* **105**(22), 227403 (2010).
13. N. Meinzer, M. Ruther, S. Linden, C. M. Soukoulis, G. Khitrova, J. Hendrickson, J. D. Olitzky, H. M. Gibbs, and M. Wegener, "Arrays of Ag split-ring resonators coupled to InGaAs single-quantum-well gain," *Opt. Express* **18**(23), 24140–24151 (2010).
14. N. Meinzer, M. König, M. Ruther, S. Linden, G. Khitrova, H. M. Gibbs, K. Busch, and M. Wegener, "Distance-dependence of the coupling between split-ring resonators and single-quantum-well gain," *Appl. Phys. Lett.* **99**(11), 111104 (2011).
15. D. J. Bergman and M. I. Stockman, "Surface Plasmon Amplification by Stimulated Emission of Radiation: Quantum Generation of Coherent Surface Plasmons in Nanosystems," *Phys. Rev. Lett.* **90**(2), 027402 (2003).

15. M. I. Stockman, "Spasers explained," *Nat. Photonics* **2**(6), 327–329 (2008).
16. R. F. Oulton, V. J. Sorger, T. Zentgraf, R.-M. Ma, C. Gladden, L. Dai, G. Bartal, and X. Zhang, "Plasmon lasers at deep subwavelength scale," *Nature* **461**(7264), 629–632 (2009).
17. M. A. Noginov, G. Zhu, A. M. Belgrave, R. Bakker, V. M. Shalae, E. E. Narimanov, S. Stout, E. Herz, T. Suteewong, and U. Wiesner, "Demonstration of a spaser-based nanolaser," *Nature* **460**(7259), 1110–1112 (2009).
18. A. E. Siegman, *Lasers* (University Science, Sausalito, CA, 1986), Chaps. 2, 3, 6, and 13.
19. The pumping rate is equivalent to a pump intensity. The pump power density is equal to  $\hbar \omega_a P_g N_0$ , and the pump intensity  $I_p = (\text{pump power})/(\text{surface area}) = \hbar \omega_a P_g N_0 (\text{volume})/(\text{surface area}) = \hbar \omega_a P_g N_0 d$ , and  $d$  is the thickness of the gain layer. If we use the numbers of our simulations,  $P_g = 3 \times 10^9 \text{ s}^{-1}$ ,  $N_0 = 5 \times 10^{23} \text{ m}^{-3}$ ,  $\omega_a = 2\pi \times 175 \text{ THz}$ , and  $d = 20 \text{ nm}$ , then  $I_p = 3.5 \text{ W/mm}^2$ .
20. A. Taflove, *Computational Electrodynamics: The Finite Difference Time Domain Method* (Artech House, London, 1995), Chaps. 3, 6, and 7.
21. A. Fang, T. Koschny, and C. M. Soukoulis, "Lasing in metamaterial nanostructures," *J. Opt.* **12**(2), 024013 (2010).

## 1. Introduction

The field of metamaterials has seen spectacular progress [1–3]. Most metamaterials have a metal-based nanostructure and eventually suffer from conductor losses at optical frequencies, which are still orders of magnitude too large for realistic applications. In addition, metamaterials' losses become an increasingly important issue when moving from multiple metal-based metamaterial layers to the bulk case [2]. Thus, the need for reducing or even compensating for the losses is a key challenge for metamaterials' technologies. One promising way of overcoming the losses is based on introducing the gain material to the metamaterial. The idea of the combination of a metamaterial with an optical gain material has been investigated by several theoretical [4–8] and experimental studies [9–13]. From the experimental point of view, the realistic gain can be experimentally realized with fluorescent dyes [9], quantum dots [10,11] or semiconductor quantum wells [12,13]. All these loss compensations are mainly attributed to the coupling between the metamaterial and the gain medium. Without sufficient coupling, the transmitted signal may be slightly amplified due to the presence of the gain medium, but no reduction of the metamaterial resonator damping can happen. Therefore, it is of vital importance to understand the mechanism of the coupling between the metamaterial and the gain medium. In addition, these ideas can be used in plasmonics to incorporate gain [14,15] to obtain new nanoplasmonic lasers [16,17,8].

In this work, we present a systematic theoretical model for pump-probe experiments of metallic metamaterials (split-ring resonators (SRRs), inversed SRRs [10,11] and fishnets [9]) coupled with the gain material, described by a generic four-level atomic system. We describe the dynamical processes in metamaterials with gain; increasing the gain changes the metamaterial properties, and we need to have self-consistent calculations [4–8] to reach a steady state. The pump-probe results affect the time dependence of the population inversion and the electric field enhancement that increases the effective gain. We find that the differential transmission  $\Delta T/T$  can be negative for SRRs on the top of the gain substrate, which is not expected [7], although  $\Delta T/T$  is positive for the gain substrate alone. These simulations [7] agree with pump-probe experiments [12,13] and can help to design (SRRs, inverse SRRs and fishnets) new experiments to compensate for the losses of metamaterials.

## 2. Theoretical model for pump-probe experiments

We model the dispersive Lorentz active medium using a generic four-level atomic system. The population density in each level is given by  $N_i (i = 0, 1, 2, 3)$ . The time-dependent Maxwell's equations for isotropic media are given by  $\nabla \times \mathbf{E}(\mathbf{r}, t) = -\partial \mathbf{B}(\mathbf{r}, t) / \partial t$  and  $\nabla \times \mathbf{H}(\mathbf{r}, t) = \partial \mathbf{D}(\mathbf{r}, t) / \partial t$ , where  $\mathbf{B}(\mathbf{r}, t) = \mu \mu_0 \mathbf{H}(\mathbf{r}, t)$ ,  $\mathbf{D}(\mathbf{r}, t) = \epsilon \epsilon_0 \mathbf{E}(\mathbf{r}, t) + \mathbf{P}(\mathbf{r}, t)$  and  $\mathbf{P}(\mathbf{r}, t)$  is the dispersive electric polarization density that corresponds to the transitions between two atomic levels,  $N_1$  and  $N_2$ . The vector  $\mathbf{P}$  introduces gain in Maxwell's equations and its time evolution can be shown to follow that of a homogeneously broadened Lorentzian oscillator

driven by the coupling between the population inversion and external electric field [12]. Thus,  $\mathbf{P}$  obeys the equation of motion

$$\frac{\partial^2 \mathbf{P}(\mathbf{r}, t)}{\partial t^2} + \Gamma_a \frac{\partial \mathbf{P}(\mathbf{r}, t)}{\partial t} + \omega_a^2 \mathbf{P}(\mathbf{r}, t) = -\sigma_a \Delta N(\mathbf{r}, t) \mathbf{E}(\mathbf{r}, t) \quad (1)$$

where  $\Gamma_a$  stands for the linewidth of the atomic transitions at  $\omega_a$  and accounts for both the nonradiative energy decay rate, as well as dephasing processes that arise from incoherently driven polarizations. In the following simulations, this value is equal to  $2\pi \times 20 \times 10^{12}$  rad/s.  $\sigma_a$  is the coupling strength of  $\mathbf{P}$  to the external electric field and its value is taken to be  $10^{-4}$  C<sup>2</sup>/kg. The factor  $\Delta N(\mathbf{r}, t) = N_2(\mathbf{r}, t) - N_1(\mathbf{r}, t)$  is the population inversion between level 2 and level 1 that drives the polarization  $\mathbf{P}$ . In order to do pump-probe experiments numerically we first pump the gain material with a short, intense Gaussian pump pulse. After a suitable time delay we probe the structure with a weak probe pulse (see Fig. 1).

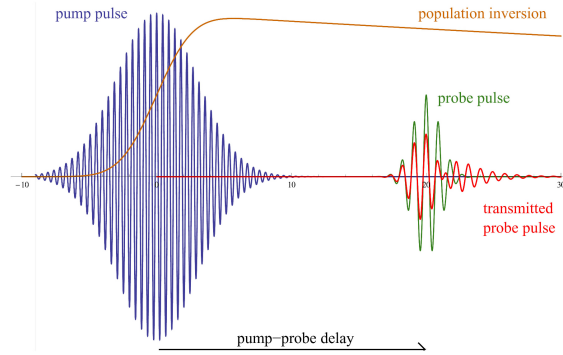


Fig. 1. Schematic illustration of pump-probe experiments.

In our model, an external mechanism pumps electrons from the ground state level  $N_0$  to the third level  $N_3$  using a gaussian pumping  $P_g(t)$ , which is proportional to the pumping intensity in the experiments. After a short lifetime  $\tau_{32}$  the electrons transfer non-radiatively into the metastable second level  $N_2$ . The second level ( $N_2$ ) and the first level ( $N_1$ ) are called the upper and lower lasing levels. Electrons can be transferred from the upper to the lower lasing level by spontaneous and stimulated emission. At last, electrons transfer quickly and non-radiatively from the first level ( $N_1$ ) to the ground state level ( $N_0$ ). The lifetimes and energies of the upper and lower lasing levels are  $\tau_{21}$ ,  $E_2$  and  $\tau_{10}$ ,  $E_1$  respectively. The center frequency of the radiation is  $\omega_a = (E_2 - E_1)/\hbar$  which is a controlled variable chosen according to each individual pump-probe experiment. The parameters  $\tau_{32}$ ,  $\tau_{21}$ , and  $\tau_{10}$  are chosen to be 0.05 ps, 80 ps and 0.05 ps respectively, which are values typical to real gain media, so that in combination with the rest parameters ( $\Gamma_a$ ,  $\sigma_a$ ,  $\omega_a$ ,  $\epsilon$ ) our results are comparable to the experiments [9–13]. The initial electron density is  $N_0(\mathbf{r}, t=0) = 5 \times 10^{23} \text{ m}^{-3}$ , with  $N_i(\mathbf{r}, t=0) = 0 \text{ m}^{-3}$  ( $i=1,2,3$ ). Thus, the atomic population densities [18] obey the following rate equations:

$$\frac{\partial N_3(\mathbf{r}, t)}{\partial t} = P_g(t) N_0(\mathbf{r}, t) - \frac{N_3(\mathbf{r}, t)}{\tau_{32}} \quad (2)$$

$$\frac{\partial N_2(\mathbf{r}, t)}{\partial t} = \frac{N_3(\mathbf{r}, t)}{\tau_{32}} + \frac{1}{\hbar \omega_a} \mathbf{E}(\mathbf{r}, t) \cdot \frac{\partial \mathbf{P}_a(\mathbf{r}, t)}{\partial t} - \frac{N_2(\mathbf{r}, t)}{\tau_{21}} \quad (3)$$

$$\frac{\partial N_1(\mathbf{r}, t)}{\partial t} = \frac{N_2(\mathbf{r}, t)}{\tau_{21}} - \frac{1}{\hbar\omega_a} \mathbf{E}(\mathbf{r}, t) \cdot \frac{\partial \mathbf{P}_a(\mathbf{r}, t)}{\partial t} - \frac{N_1(\mathbf{r}, t)}{\tau_{10}} \quad (4)$$

$$\frac{\partial N_0(\mathbf{r}, t)}{\partial t} = \frac{N_1(\mathbf{r}, t)}{\tau_{10}} - P_g(t) N_0(\mathbf{r}, t) \quad (5)$$

where the Gaussian pump is  $P_g(t) = P_0 \times e^{-(t-t_p)^2/t_p^2}$ , with  $t_p = 6$  ps [19],  $\tau_p = 0.15$  ps and  $P_0$  ranging from  $1 \times 10^9$  s<sup>-1</sup> to  $29 \times 10^9$  s<sup>-1</sup>, depending on the individual configuration. In order to solve the response of the active materials in the electromagnetic fields numerically, the FDTD technique is utilized [20], using an approach similar to the one outlined in [21].

### 3. Structure description and results

#### 3.1. Three different U-Shape SRR Structures

The structure considered is a U-Shape SRR fabricated on a gain-GaAs substrate [7,12,13] with a square periodicity of  $p = 250$  nm (see Fig. 2(a)). The SRR is made of silver with its permittivity modeled by a Drude response:  $\epsilon(\omega) = 1 - \omega_p^2/(\omega^2 + i\omega\gamma)$ , with  $\omega_p = 1.37 \times 10^{16}$  rad/s and  $\gamma = 2.73 \times 10^{13}$  rad/s. The incident wave propagates perpendicular to the SRR plane and has the electric field polarization parallel to the gap (see Fig. 2(a)). The corresponding geometrical parameters are  $a = 150$  nm,  $h_d = 40$  nm,  $h_g = 20$  nm,  $h_s = 30$  nm,  $w = 50$  nm and  $h = 75$  nm.

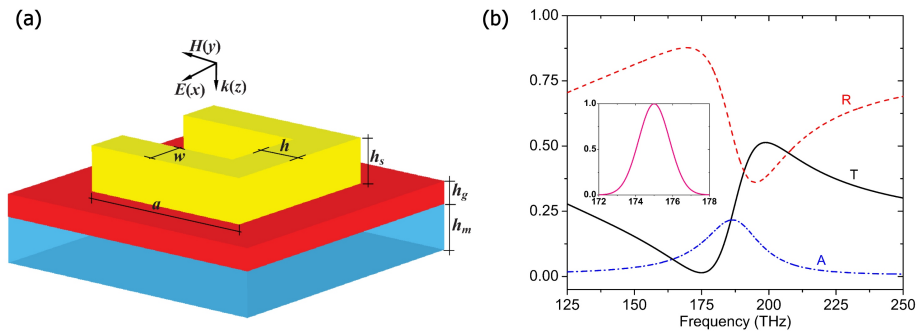


Fig. 2. (a) Schematic of the unit cell for the silver-based SRRs structure (yellow) with the electric field polarization parallel to the gap. The dielectric constants  $\epsilon$  for gain (red) and GaAs (light blue) are 9.0 and 11.0, respectively. (b) Calculated spectra for transmittance  $T$  (black), reflectance  $R$  (red), and absorbance  $A$  (blue) for the structure shown in Fig. 2(a). The inset shows the profile of the probe pulse with a center frequency of 175 THz (FWHM = 2 THz).

Figure 2(b) shows the calculated spectrum (without pump) of transmittance  $T$ , reflectance  $R$  and absorbance  $A$  for the structure shown in Fig. 2(a). The resonant frequency is around 175 THz, and we refer to the resonant frequency according to the dip in the transmittance. The reason for this choice lies in the fact that we are interested in how the interaction of the gain system with the metamaterial may lead to a less damped oscillator, ideally undamped. As such, the unpumped oscillator is expected to exhibit increased impedance mismatch with the exterior close to its eigenfrequency (maximum of oscillator absorption) and consequently a dip in the transmittance. For comparison, we also introduce two other gain configurations (see Fig. 3), where the gain is embedded in the gap of the SRR (Fig. 3(a)) and the SRR is embedded in the gain with 50 nm in height (Fig. 3(b)). The dimensions and simulated parameters are kept the same as in Fig. 2(a), except for the gain material permittivity which is set to  $\epsilon = 1$ , in order to keep the resonance frequency fixed at 175 THz for all three systems.

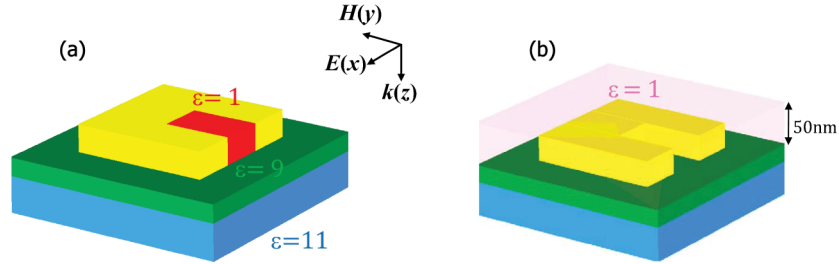


Fig. 3. The structure and the corresponding parameters. The gain material, which is denoted by the areas with  $\epsilon = 1$  is located (a) in the gap, and (b) above the structure. In these configurations, we have changed the permittivity of the gain material in order to fix the resonance frequency at 175 THz, and here we only consider the perpendicular incidence case.

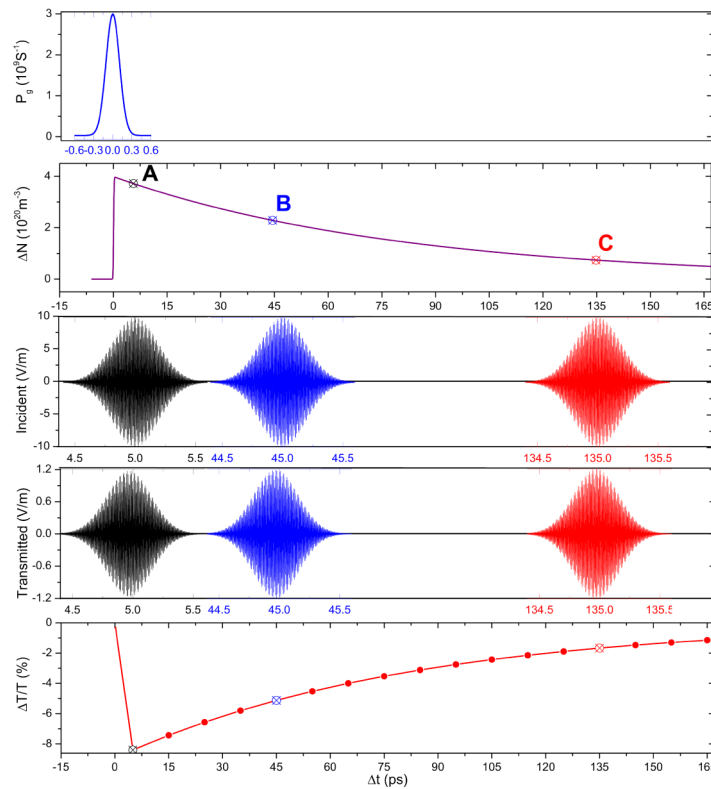


Fig. 4. Schematic of the numerical pump-probe experiments [12,13] for the case on resonance. The results correspond to the geometry of Fig. 2(a) with  $\epsilon = 9$ , accounting for quantum wells as the gain medium, as in [12]. From the top to the bottom, each row corresponds to the pump pulse, population inversion, incident signal (with time delays 5, 45, and 135 ps), transmitted signal, and differential transmittance  $\Delta T/T$ . It should be mentioned here that the incident frequency of the probe pulse is 175 THz with a FWHM of 2 THz and is equal to the SRR resonance frequency.

In our analysis, we first pump the active structure (see Fig. 2(a) and Fig. 3) with a short intensive Gaussian pump pulse  $P_g(t)$  (see Fig. 4, top panel). After a suitable time delay (i.e. the pump-probe delay), we probe the structure (see Fig. 2(a) and Fig. 3) with a weak Gaussian probe pulse with a center frequency close to the SRR resonance frequency of 175 THz. The incident electric field amplitude of the probe pulse is 10 V/m, which is well inside the linear response regime. Then, we can Fourier transform the incident probe pulse to obtain the

spectral transmittance of the system as seen by the probe pulse. Additionally, we obtain the total pulse transmittance by dividing the energy in the transmitted pulse by the energy in the incident pulse, integrated in the time domain. We define the difference transmittance  $\Delta T/T$  by taking the difference of the measured total plus transmittance with pumping the active structure minus the same without pumping and dividing it by the total plus transmittance without pumping. This difference is a function of the pump-delay. The bottom panel in Fig. 4 gives a differential  $\Delta T/T$  which is negative [7] and agrees with the experiments [12,13]. Figure 5 shows the results for the difference in absorptance ( $\Delta A$ ), difference in reflectance ( $\Delta R$ ), their sum ( $\Delta A + \Delta R$ ) and the difference in transmittance [ $\Delta T = -(\Delta A + \Delta R)$ ] between pump ( $P_0 = 3 \times 10^9 \text{ s}^{-1}$  solid black, multiply by 6,  $P_0 = 29 \times 10^9 \text{ s}^{-1}$  dotted black) and no pump using a wide probe (FWHM = 54 THz) pulse with a fixed pump-probe delay of 5 ps.

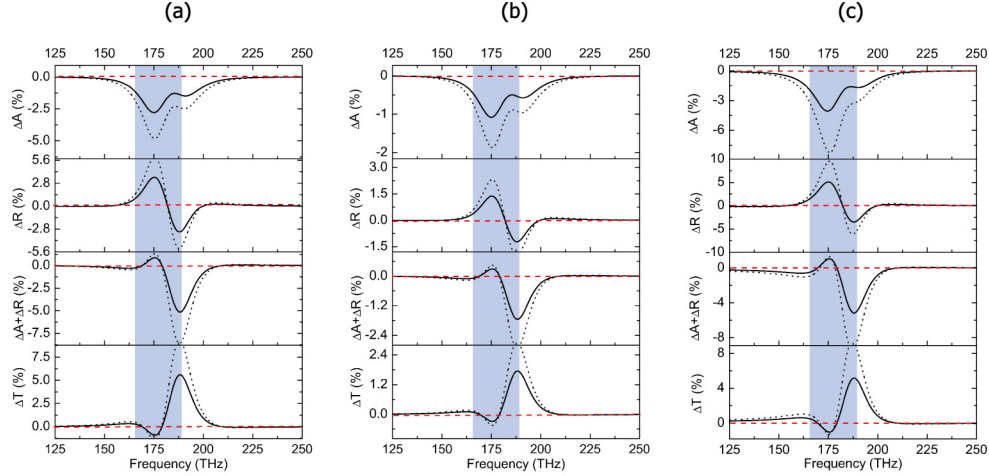


Fig. 5. Results of spectrum difference for three different designs with pumping rate  $3 \times 10^9 \text{ 1/s}$  (solid black, multiplied by 6) and  $29 \times 10^9 \text{ 1/s}$  (dotted black). (a) gain underneath, (b) gain in gap, and (c) gain above the structure. The shaded area corresponds to the spectral range examined in Fig. 6.

The results of Fig. 5 are obtained for pump-probe experiments in the three different gain/SRR structures with the probe frequency equal to the resonance frequency of the SRRs (175 THz). Notice that  $\Delta R$  is positive,  $\Delta A$  is negative and  $\Delta T$  is also negative very close to the resonance frequency. If the probe center frequency moves away from the SRR resonance frequency, the negative  $\Delta T/T$  decreases in magnitude, and finally  $\Delta T/T$  becomes positive. This is a clear indication that the gain material couples with the SRR, as the coupling at their common resonance frequency leads to reduction of the SRR damping and consequently to a stronger and narrower resonance, thus increased impedance mismatch close to the resonance frequency and increased reflection; hence to reduced transmittance, which increases again as we move away from this spectral region, eventually becoming positive. These results for  $T$  and  $\Delta T/T$  are also shown in Fig. 6 for the gain configurations of Fig. 3(a), Fig. 3(b) (in Fig. 6(a) the gain is embedded in the gap of the SRR, in Fig. 6(b) the SRR is embedded in the gain with 50 nm in height). At the resonance frequency, 175 THz, when the magnitude of the Gaussian pump pulse is  $P_0 = 3 \times 10^9 \text{ s}^{-1}$ ,  $\Delta T/T = -5\%$  (Fig. 6(a)) and  $\Delta T/T = -22\%$  (Fig. 6(b)).

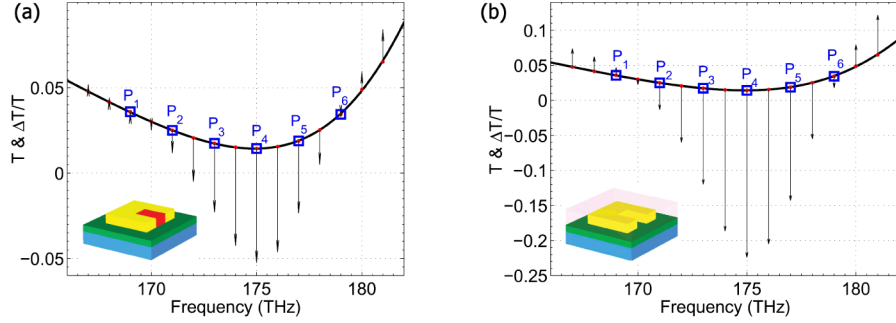


Fig. 6. The transmittance  $T$  (without pump, solid line) and the on-resonance differential transmittance  $\Delta T/T$  results (vector arrow) for the SRRs with (a) gain in gap and (b) gain above the structure. The direction and the length of the arrow stand for the sign and the amplitude of  $\Delta T/T$ , respectively. The squares from  $(P)_1$  to  $(P)_6$  correspond to the frequency of probe pulse ranging from 169 to 179 THz with uniform step of 2 THz.

### 3.2. The plasmonic inverse SRR

The inverse SRR is made of gold with its permittivity modeled by a Drude response:  $\epsilon(\omega) = \epsilon_\infty - \omega_p^2 / (\omega^2 + i\omega\gamma)$ , with  $\epsilon_\infty = 9.6$ ,  $\omega_p = 1.372 \times 10^{16}$  rad/s and  $\gamma = 10.68 \times 10^{13}$  rad/s. The gain material has a dielectric constant of  $\epsilon_g = 2.2$ , which corresponds to an averaged permittivity of PbS quantum dots dispersed in a PMMA solution (purple region in Fig. 7(a)), as in [11]. The incident wave propagates perpendicular to the SRR plane and has the electric field polarization parallel to y-axis (see Fig. 7(a)). Figure 7(b) shows the calculated spectrum (without pump) of transmittance  $T$ , reflectance  $R$  and absorptance  $A$  for the structure shown in Fig. 7(a). The resonant frequency is around 214 THz and we refer to the resonant frequency according to the dip of the transmittance.

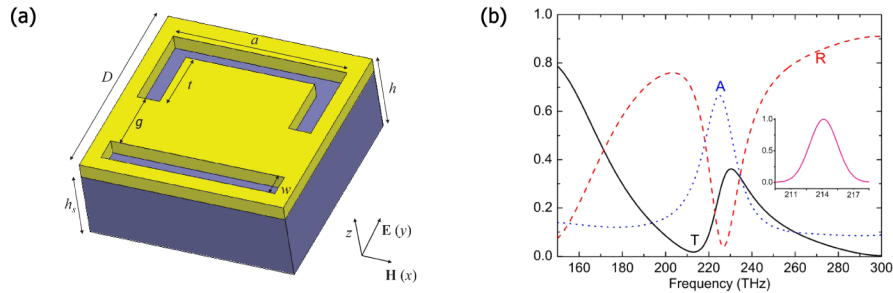


Fig. 7. (a) Schematic of a plasmonic metamaterial functionalized with gain material ( $\epsilon_g = 2.2$ ). Feature sizes: unit cell  $D = 545$  nm, horizontal slit  $a = 470$  nm, unit length  $h = 230$  nm,  $h_s = 180$  nm, top vertical slit and gap  $t = g = 170$  nm, and slit width  $w = 65$  nm. Also, there is an additional 400 nm glass substrate on the top of the structure with  $\epsilon_{sub} = 2.56$ . The metamaterial is made of gold with its permittivity modeled by a Drude response. (b) Calculated spectra for transmittance  $T$  (black), reflectance  $R$  (red), and absorptance  $A$  (blue) for the structure shown in Fig. 7(a). The inset shows the profile of the probe pulse with a center frequency of 214 THz (FWHM = 3 THz).

Figure 8 gives an overview of the results obtained for the case of inversed SRR [10,11] on resonance, i.e.  $\omega_a = 2\pi \times 214 \times 10^{12}$  rad/s. Data for the structure in Fig. 7(a) is given in Fig. 8. For parallel polarization, the light does couple to the fundamental inversed SRR resonance. In Fig. 8(a) the system is pumped with  $P_0 = 3 \times 10^9$  s $^{-1}$  and the probe center frequency increases from top (205 THz) to bottom (223 THz).

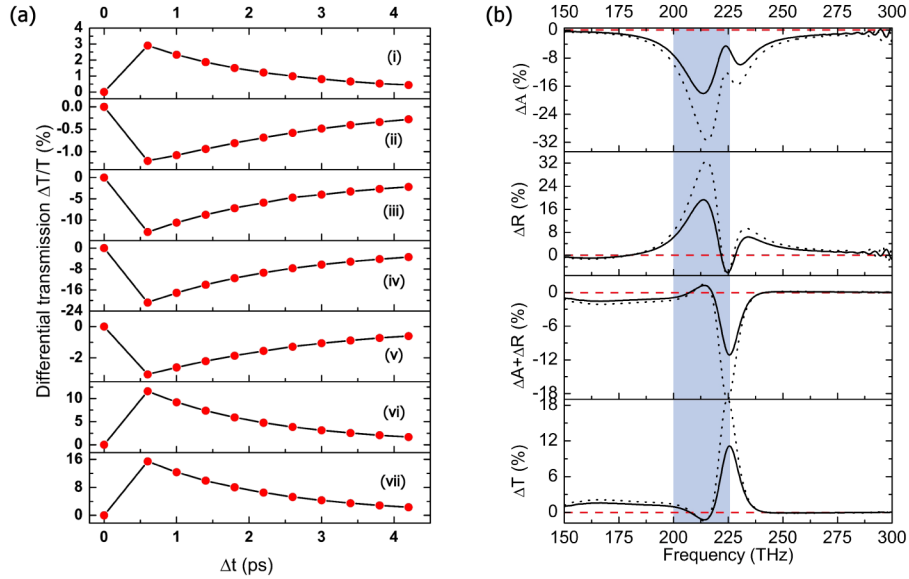


Fig. 8. (a) Calculated time domain results of  $\Delta T/T$  for the inverse SRR structure with pumping rate  $3 \times 10^9$  1/s. (i) to (vii) correspond to the probe frequency ranging from 205 THz to 223 THz with uniform step of 3 THz. (b) Results of spectrum difference with pumping rate  $1 \times 10^9$  1/s (solid black) and  $4 \times 10^9$  1/s (dotted black) for pump-probe delay of 0.6ps. The small ripples around 300THz are numerical artifacts due to the limited bandwidth of the probe pulse (54THz). The shaded area corresponds to the spectral range examined in Fig. 9.

Note that the width of the probe spectrum is 3 THz (see the inset in Fig. 7(b)). Hence, the data have been taken with 3 THz spectral separation.  $\Delta T/T$  reaches values negative as  $-22\%$  around  $f_{probe} = 214$  THz. Additionally, we may also have positive  $\Delta T/T$  at the very edges of the probe range (see in Fig. 8(i) = 205 THz and Fig. 8(vii) = 223 THz), as observed with the previous SRRs systems. Figure 8(b) shows the results for the difference in absorbance ( $\Delta A$ ), difference in reflectance ( $\Delta R$ ), their sum ( $\Delta A + \Delta R$ ) and the difference in transmittance [ $\Delta T = -(\Delta A + \Delta R)$ ] between pump ( $P_0 = 1 \times 10^9$  s $^{-1}$  solid black,  $P_0 = 4 \times 10^9$  s $^{-1}$  dotted black) and no pump using a wide probe (FWHM = 54 THz) pulse with a fixed pump-probe delay of 0.6 ps. These results for  $T$  and  $\Delta T/T$  are also shown in Fig. 9 for  $P_0 = 1 \times 10^9$  s $^{-1}$ . In this case, at the resonance frequency, 214 THz,  $\Delta T/T = -20\%$ .

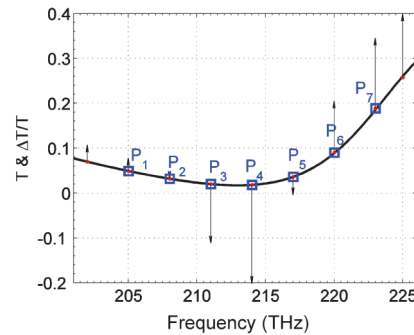


Fig. 9. The transmittance  $T$  (without pump, solid line) and the on-resonance differential transmittance  $\Delta T/T$  results (vector arrow) for the inverse SRR structure with pumping rate  $1 \times 10^9$  1/s. The direction and the length of the arrow stand for the sign and the amplitude of  $\Delta T/T$ , respectively. The squares from (P)<sub>1</sub> to (P)<sub>7</sub> correspond to the frequency of probe pulse ranging from 205 to 223 THz with uniform step of 3 THz.

### 3.3. The fishnet structure

The configuration and corresponding parameters of the fishnet structure in simulations are shown in Fig. 10. Figure 10(b) shows the calculated spectrum (without pump) of transmittance  $T$ , reflectance  $R$  and absorptance  $A$  for the structure shown in Fig. 10(a). The resonant frequency is around 495 THz, and we refer to the resonant frequency according to the peak of the transmittance.

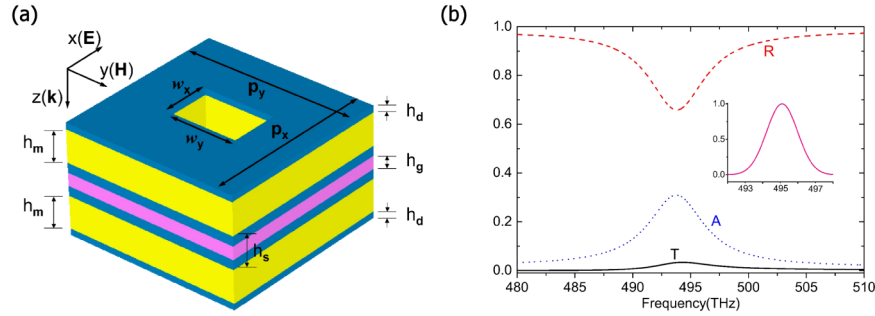


Fig. 10. Unit cell ( $p_x = p_y = 280$  nm) of the perforated fishnet structure with gain embedded in-between two metal (silver) layers. The geometric parameters are  $w_x = 75$  nm,  $w_y = 115$  nm,  $h = 170$  nm,  $h_m = h_s = 50$  nm,  $h_d = 10$  nm and  $h_g = 20$  nm. The thicknesses of the silver (yellow) and gain (magenta) layer are  $h_m$  and  $h_g$ , respectively. The dielectric layer (blue) and the gain have a refractive index  $n = 1.65$ . (b) Calculated spectra for transmittance  $T$  (black), reflectance  $R$  (red), and absorptance  $A$  (blue) for the structure shown in Fig. 10(a). The inset shows the profile of the probe pulse with a center frequency of 495 THz (FWHM = 2 THz).

Figure 11 shows the results for the difference in absorptance ( $\Delta A$ ), difference in reflectance ( $\Delta R$ ), their sum ( $\Delta A + \Delta R$ ) and the difference in transmittance [ $\Delta T = -(\Delta A + \Delta R)$ ] between pump ( $P_0 = 1.7 \times 10^9$  s $^{-1}$ ) and no pump using a wide probe (FWHM = 54 THz) pulse with a fixed pump-probe delay of 5 ps.

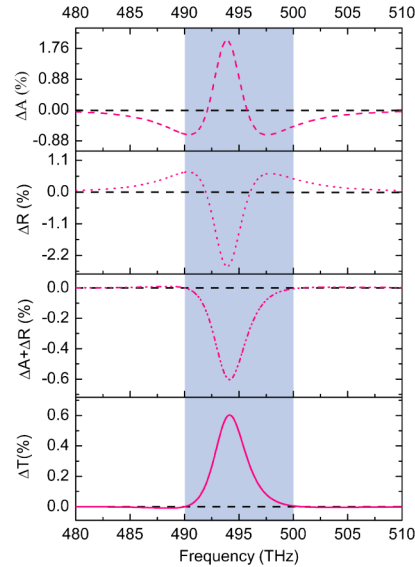


Fig. 11. Frequency domain numerical pump-probe experiments results for the fishnet structure. Simulations results for the differences in transmittance ( $\Delta T$ ), reflectance ( $\Delta R$ ), and absorptance ( $\Delta A$ ) versus frequency with pumping rate  $1.7 \times 10^9$  1/s. The shaded area corresponds to the spectral range examined in Fig. 12.

This configuration is fundamentally different from the previous ones, as in addition to  $\epsilon$ ,  $\mu$  is also negative at the resonance frequency and therefore we have a transmission peak near the resonance rather than a dip. Undamping and narrowing the metamaterial resonance can, in this case, actually reduce the impedance mismatch and, therefore, we may observe a positive differential transmittance  $\Delta T > 0$  [9]. Apparently the increase of transmittance due to the contribution from gain is stronger than the reduction imposed by the metamaterial undamping. In total, the transmittance increases as opposed to the previous configurations. In Fig. 12, the transmittance  $T$  (without pump, solid line) and the on-resonance differential transmittance  $\Delta T/T$  results (vector arrows) are shown. In the fishnet structure  $\Delta T/T$  is positive and our simulations have verified that the coupling between the metamaterial resonance and the gain medium is dominated by near-field interactions. Our simulations in the fishnet structure with gain medium can be used for new pump-probe experiments to compensate for the losses of fishnet metamaterials.

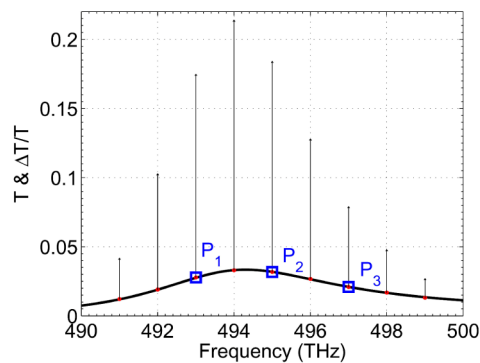


Fig. 12. The transmittance  $T$  (without pump, solid line) and the on-resonance differential transmittance  $\Delta T/T$  results (vector arrow) for the fishnet structure with pumping rate  $1.7 \times 10^9$  1/s. The direction and the length of the arrow stand for the sign and the amplitude of  $\Delta T/T$ , respectively. The squares from  $(P)_1$  to  $(P)_3$  correspond to the frequency of probe pulse ranging from 493 to 497 THz with uniform step of 2 THz.

#### 4. Conclusion

In this work we have presented a systematic theoretical model for pump-probe experiments of metallic metamaterials coupled with the gain material, described by a generic four-level atomic system. We investigated three characteristic metamaterial configurations, namely SRRs, inversed SRRs and fishnets. In all cases we observed strong coupling between the gain material and the metamaterial, which, for the case of on-resonance, leads the differential transmission of the combined system to differ significantly from that of the bare gain system. Using pump-probe simulations, we find a distinct behavior for  $\Delta T/T$  of the probe pulse, which is negative for the SRR configurations and positive for the fishnet metamaterial. This is a clear indication of reduction of the resonator damping and is hence promising for loss reduction in such systems or even full loss compensation. Our model can be used to design new pump-probe experiments to compensate for the losses of metamaterials.

#### Acknowledgments

Work at Ames Lab was partially supported by the U.S. Dept. of Energy, Basic Energy Science, Materials Science and Engineering, Contract no. DE-AC02-07CH11358. Simulation work at FORTH (theory) was supported by the European Research Council under the ERC Advanced Grant no. 320081 (PHOTOMETA).